Efficient electricity storage with a battolyser, an integrated Ni-Fe battery and electrolyser

Mulder, F. M.; Weninger, B. M.H.; Middelkoop, J.; Ooms, F. G.B.; Schreuders, H.

DOI
10.1039/c6ee02923j

Publication date
2017

Document Version
Accepted author manuscript

Published in
Energy & Environmental Science

Energy & Environmental Science

PAPER

Efficient electricity storage with a battolyser, an integrated Ni–Fe battery and electrolyser†

Cite this: DOI: 10.1039/c6ee02923j

F. M. Mulder,*[a] B. M. H. Weninger,[a] J. Middelkoop,[a] F. G. B. Ooms[b] and H. Schreuders[a]

Received 7th October 2016,
Accepted 14th December 2016

DOI: 10.1039/c6ee02923j

www.rsc.org/ees

Grid scale electricity storage on daily and seasonal time scales is required to accommodate increasing amounts of renewable electricity from wind and solar power. We have developed for the first time an integrated battery-electrolyser ('battolyser') that efficiently stores electricity as a nickel–iron battery and can split water into hydrogen and oxygen as an alkaline electrolyser. During charge insertion the $Ni(OH)_2$ and $Fe(OH)_2$ electrodes form nanostructured NiOOH and reduced Fe, which act as efficient oxygen and hydrogen evolution catalysts respectively. The charged electrodes use all excess electricity for efficient electrolysis, while they can be discharged at any time to provide electricity when needed. Our results demonstrate a remarkable constant and a high overall energy efficiency (80–90%), enhanced electrode storage density, fast current switching capabilities, and a general stable performance. The battolyser may enable efficient and robust short-term electricity storage and long-term electricity storage through production of hydrogen as a fuel and feedstock within a single, scalable, abundant element based device.

Broader context

Electricity storage in batteries and artificial hydrogen fuels is key to enable the implementation of renewable energy from intermittent solar and wind power. This calls for both environmentally sound and durable batteries and electrolysers. Here, we design an integrated battery and electrolyser in one novel device based on electrodes that contain the abundant elements Ni and Fe as active elements. The battery – electrolyser operates efficiently as a battery and when fully charged as an electrolyser. It is remarkable that the electrodes form and reform the active battery materials $Ni(OH)_2$ and $Fe(OH)_2$ during discharge even after long term electrolysis. The oxygen evolution catalyst NiOOH and the hydrogen evolution catalyst of reduced Fe are formed automatically during charge. The operation is shown to be up to 90% energy efficient, highly durable and flexible, where the electrolysis also protects intrinsic battery overcharge. The flexibility is such that it enables storing electricity for a short term, therefore circumventing conversions to fuel and back, while also enabling conversion to fuel for long term storage. The materials efficiency of integrating two applications in one is high, which is an additional environmental benefit.

Introduction

In a renewable energy future the storage of electricity in batteries[1,2] and in the production of hydrogen fuels[3,4] will be required to come to adequate energy availability on both daily and seasonal timescales.[5,6] Batteries will be used for short-term energy efficient storage while long-term storage requires hydrogen fuels at the expense of conversion losses when generating electricity afterwards. The typical volume of energy stored for various days in a year may range from equal amounts of battery storage and fuel generation (summer), to the whole capacity only as battery storage (autumn–spring).[6] The storage infrastructure should provide for these different requirements throughout the year, and support the 'storage merit order' of first efficient battery storage, and second less efficient fuel production, storage and conversion. The battolyser presented here integrates the functionality of the Ni–Fe battery[7,8] and the alkaline electrolyser[9–12] in one flexible, switchable and efficient solution. Most remarkably the battery electrodes and the hydrogen and oxygen evolution catalysts are formed and reformed over many charge and discharge cycles while there is excellent battery reversibility after prolonged charge insertion and electrolysis. It may provide an optimal utilisation factor throughout the year, by storing and providing electricity, and converting excess electricity far beyond the battery capacity to hydrogen.

[a] Technische Universiteit Delft Faculteit Technische Natuurwetenschappen, Chemical Engineering, Delft, Netherlands
[b] Technische Universiteit Delft Faculteit Technische Natuurwetenschappen, RST, Delft, Netherlands

† Electronic supplementary information (ESI) available. See DOI: 10.1039/c6ee02923j

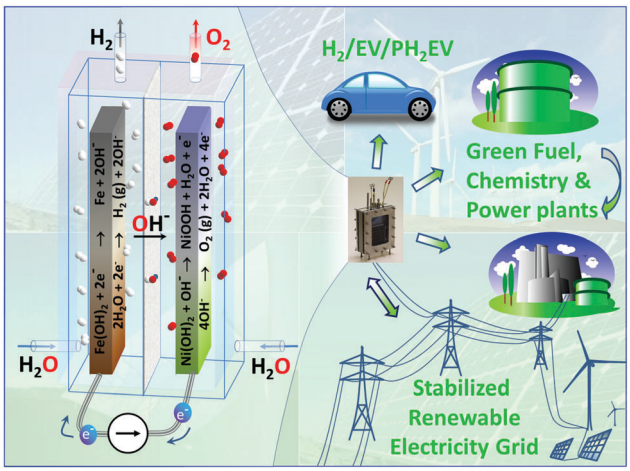

Fig. 1 Battolyser functionality and application areas. (left) Integrated electrochemical battery and electrolyser (battolyser) layout. During charge the Ni–Fe electrodes store electricity from the electricity source, converting the electrode materials as indicated. When fully charged hydrogen and oxygen are formed by splitting water, the grey diaphragm transmits OH^- and separates O_2 and H_2. (right) Potential applications of the battolyser: as a sink and source for stabilising the electricity grid, for supplying electricity as well as H_2 as a fuel for *e.g.* plug-in hybrid electric and hydrogen vehicles (PH_2EV), and for H_2 as chemical feedstock.

The hydrogen production may enable long-term energy storage in (effectively carbon neutral) fuels and feedstock *via* chemical processes such as the Sabatier (methane from H_2 and CO_2), Haber–Bosch (ammonia synthesis from clean H_2 and N_2, which has current industrial efficiencies of above 90%[13] and provides high energy density liquid storage at room temperature (RT) and ~8.5 Bar), and Fischer–Tropsch (alkanes from CO/CO_2 and H_2) processes.

Fig. 1 illustrates the battolyser and the function it can provide in several potential application areas. The device has a negative electrode in which $Fe(OH)_2$ is reduced to Fe upon charge:

$$Fe(OH)_2 + 2e^- \xrightarrow{\text{charge}} Fe + 2OH^- \quad (1)$$

(−0.88 V relative to the standard hydrogen electrode (SHE)), considering only the Fe/Fe^{2+} discharge plateau. The positive electrode contains $Ni(OH)_2$ that upon charge releases a proton:

$$Ni(OH)_2 + OH^- \xrightarrow{\text{charge}} NiOOH + H_2O + e^- \quad (2)$$

(+0.49 V *vs.* SHE). An alkaline KOH electrolyte conducts the OH^- ions. These electrode materials are known from the robust Ni–Fe battery introduced by Jungner and Edison which has also a track record of extreme longevity.[7,8] When becoming fully charged the formed Fe and NiOOH electrodes become increasingly active as efficient hydrogen (HER) and oxygen evolution reaction (OER) catalysts at increased cell potential. Then at the positive electrode the oxygen evolution takes place:

$$4OH^- \xrightarrow{\text{overcharging}} O_2(g) + 2H_2O + 4e^- \quad (3)$$

(1.23 − 0.059 × pH *vs.* SHE) and at the negative electrode hydrogen evolution:

$$2H_2O + 2e^- \xrightarrow{\text{overcharging}} H_2(g) + 2OH^- \quad (4)$$

(0.00 − 0.059 × pH *vs.* SHE). It is known in the literature that the HER and OER catalysts are efficient in an alkaline environment indeed,[14] but here it will be shown that they are formed and reformed spontaneously during many charge, electrolysis and full discharge cycles, without apparent loss of functionality. Cyclic voltammograms of both electrodes (see ESI,† Fig. S7) are in agreement with the literature[15,16] and ascertain the reaction mechanism. A ceramic polymer composite diaphragm[11,17] separates hydrogen and oxygen gas while permitting the flow of OH^- ions between the electrodes. For construction see the ESI,† Fig. S1.

Concept of the battolyser

The integrated battery and electrolyser concept works as follows: the battery functionality provides electricity storage capacity, which is charged when a surplus of renewable electricity is available and discharged when there is an electricity deficiency. The battery functionality stores electricity directly with a high power-to-power efficiency. When the battery is reaching its designed capacity, production of hydrogen from the excess electricity larger than the battery capacity takes place, *i.e.* the combination of a battery and an electrolyser has no capacity restriction. Utilising hydrogen as storage requires a hydrogen storage method and back conversion from hydrogen to power (not considered here), which lower the overall power-to-power efficiency considerably compared to battery storage. However, hydrogen or its derived fuels are needed for seasonal energy storage since batteries are too costly to utilise only once in a season and also have much lower energy density than liquid hydrogen fuels like *e.g.* liquid ammonia or alkanes. The optimisation of the overall energy efficiency thus provides a rationale for combining efficient short term battery storage and long term hydrogen fuel storage.

The battolyser has the capability to follow electricity fluctuations caused by renewable generation or consumers demand as it allows for various charge and discharge rates. The device can operate essentially around the clock, leading to a high degree of utilization: either the electricity surplus is stored in electrical storage capacity and hydrogen or electricity is provided from the storage when there is a deficit. An illustration of potential battolyser use throughout characteristic days of the year is given in Fig. 2 in comparison with an independent battery and an electrolyser next to each other. Hydrogen will be produced at times when renewable electricity is highly available that the battery capacity is already reached and electricity prices are therefore low because of abundant supply. The battolyser will be used almost continuously while the individual battery and electrolyser will have a significantly lower utilisation or capacity factor; the electrolyser has no use hours in large periods of the year because the electricity surpluses are not larger than the battery capacity. Low utilisation factors are generally economical and from the materials use standpoint unfavourable. In principle the battolyser uses a single system instead of two separate ones which is also highly important for economic considerations.

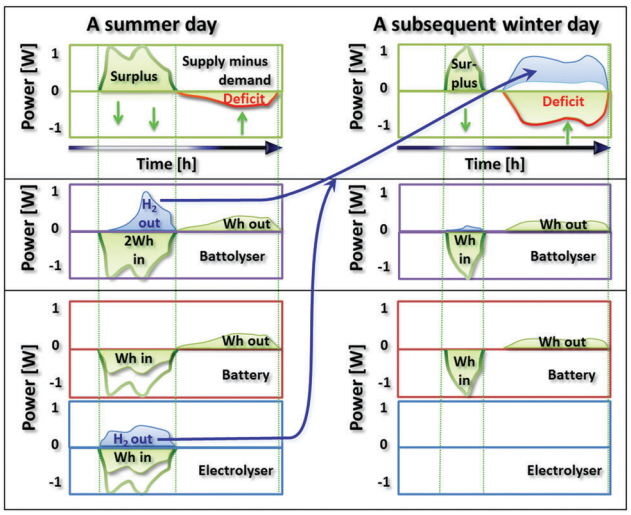

Fig. 2 Battolyser utilisation. Illustration of storage of a surplus of renewable power (top) using the battolyser (middle) or in a separate battery and electrolyser (bottom). The full power (indicated by W) and energy (W h) capacities are a hardware choice that needs to provide the necessary power and energy storage handling capabilities during different days throughout the year. On the left summer day there is both short-term (green area) and long-term (blue H_2 area) storage; in autumn, winter or spring, the full surplus energy and power may go into short term storage only because one requires the power a few hours later (and one prevents conversion to fuel since conversion means higher energy losses).[6] The indicated daily deficits are compensated by short-term battery capacity (on this summer day) and by the battery plus hydrogen derived electricity (the winter day).

Results

Functionality of the battolyser

The battolyser provides a flexible storage capacity for increasing charge insertion with full intermediate discharge, see Fig. 3. Increasing electrical current insertion results in increasing battery electrode charging, and when charged, increasing electrolytic gas production. Increasing electrical current insertion far beyond the nominal cell capacity not only enables electrolytic gas production but also allows for usage of electrode materials normally not employable for battery operation, and thus yielding higher discharge capacities. Hydrogen evolution starts at small rates immediately, whereas initially no oxygen evolution is detected. This is because the Ni electrode is the limiting electrode in the battolyser cell, which means that after discharge there is almost no NiOOH available to catalyse O_2 evolution, while there is still some unreduced Fe allowing for hydrogen evolution. The normalised oxygen evolution catches up later and surpasses hydrogen evolution at about 80% of the nominal discharge capacity of the battery (C), 4 h after the start of each charge insertion. The highest gas evolution starts after the battery is charged to a nominal reversible battery discharge capacity of 10 A h (see also the Experimental section and the ESI,† Fig. S2b). Overall, stoichiometric gas evolution takes place. During discharge a fast decrease of gas evolution towards zero is observed. This is in line with earlier gas measurements of Ni–Fe batteries that were performed to characterise the

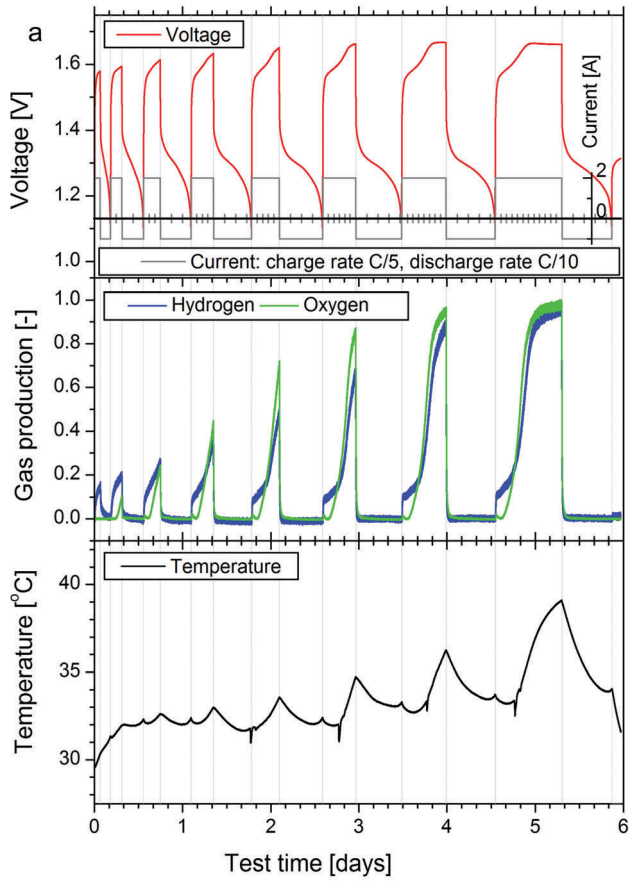

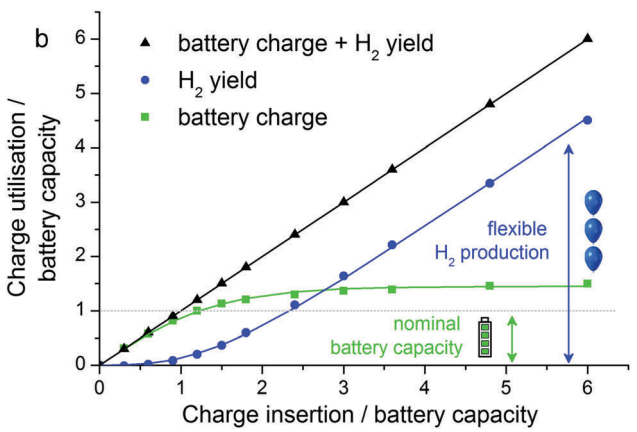

Fig. 3 Battery and electrolysis yield. (a) Top: Observed potential during constant current insertion over increasing durations, followed by full discharges to 1.1 V. (The horizontal axis includes additional grey tick-marks for charge or discharge, step size ±0.3 C) Middle: Resulting normalised hydrogen and oxygen evolution. Bottom: Temperature development for the thermally insulated cell (detailed information see ESI,† Table S2 and Fig. S9). (b) Battolyser utilisation of charge in the battery and the H_2 production divided by the nominal battery discharge capacity of C = 10 A h (now measured at a constant regulated temperature of T = 30 °C). The drawn lines are fits with eqn (9) and (10), see the Experimental section. (Detailed information see ESI,† Table S3.)

occurring gas compositions in relation to explosion risks.[18] During battery (dis-)charge or electrolysis the temperature increases when the overpotentials increase compared to the

battery open circuit potential (OCV) or the thermoneutral water splitting potential respectively (setup with a thermally insulated cell, see the Experimental section). Interestingly the gas evolution is not constant during electrolysis. We attribute this to the increasing device temperature which promotes electrolysis, leading to increased gas yield at the expense of slower battery charge.

We designed a test-series to simulate various real-life renewable electricity supply and demand situations with partial and full (dis)charging, rapid charge–discharge switching, continuous or intermittent overcharging, as well as the around the clock cycling for months. The results are shown in Fig. 4 and in the ESI,† Fig. S4. Experiments were performed in four separate cells and proved to be fully reproducible between cells. The remarkable findings in Fig. 4 are the overall stability of the energetic efficiency of 80–90% over many different types of cycles (see the ESI,† Fig. S3, for selection of performed cycles), and the stability of the reversible discharge capacities of the battery even after more than 500 deep discharges and (over-)charges to more than 1000 times the nominal capacity. On average more than 40% of the total inserted charge was used for performing electrolysis. Energetic efficiency is calculated from the sum of the energy retrieved during the cell discharge and the chemical energy from hydrogen that was produced (see the Experimental section and the ESI,† Fig. S2a). Neither the battery capacity nor the electrolysis are harmed by the many cycles that included battery overcharges up to 10 times the nominal capacity, rapid current reversals and deep discharges for each cycle. Such a finding illustrates the viability for operation as an integrated battery and electrolyser. During the test period of 18 months a single cell consumed 1451.4 g of water, where 1409.7 g (97.1%) is expected due to electrolysis, the remainder is lost *via* the humidification of the released gas. Other side reactions leading to more weight loss or to H_2O_2 formation are not observed in trace gas analysis; the total faradaic efficiency of battery charge plus water splitting is 100% within experimental accuracy (±0.5%, see the Experimental section). The cells still operate with the initial electrolyte, only demineralised water was added.

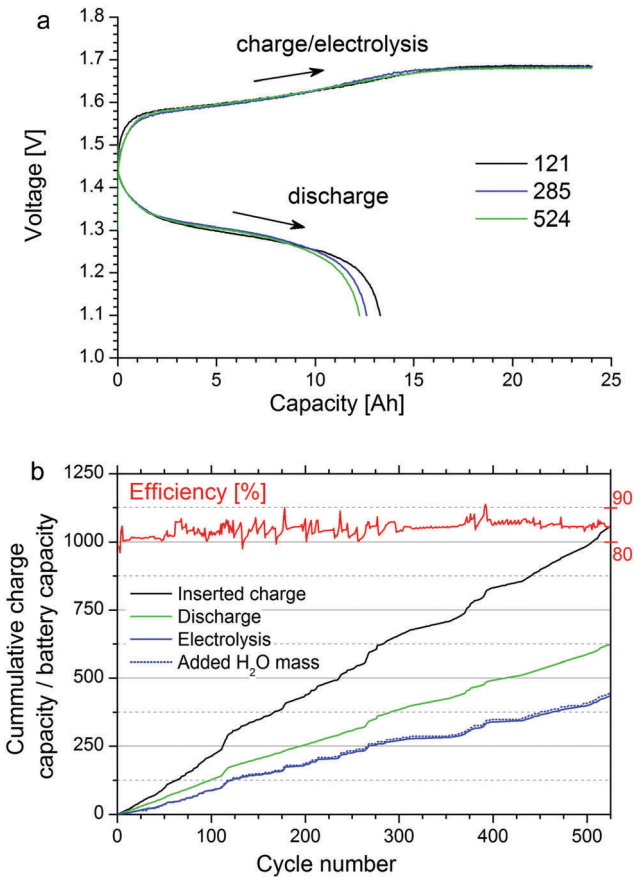

Fig. 4 Long term cycling stability and efficiencies. (a) Voltage response of a battolyser cell being charged to 24.0 A h with subsequent discharge during the indicated cycle numbers. Changes over time are a slight ~7 mV decrease of the required potential during electrolysis (increases efficiency) which causes a slightly larger fraction of the 24.0 A h to be spent on electrolysis in these cycles, and equally less on battery charge. (b) The overall energy efficiency for a large number of different experimental cycles. A cycle is counted from full discharge to full discharge with various full or partial (over/dis)charge programs in between. Consistently the overall cycle energy efficiency adds up to above 80 to 90%. (see the Experimental section and ESI,† Fig. S2–S4 for detail information). Also plotted is the cumulative inserted charge and breakdown in battery charge and electrolysis, and the required cumulative H_2O mass to replenish the electrolyte expressed with respect to the battery capacity.

The discharge capacity at an equal inserted charge of 24.0 A h is shown in Fig. 4a during the indicated cycle numbers. The slight reduction of the electrolysis potential (−7 mV) at the same applied current will cause that a larger amount of current is spent on electrolysis (see below). The change of the electrode occurs mainly in the first 285 cycles and becomes less later on; it appears to be accompanied by a slight increase of total energy efficiency with the progressing cycle number as well (Fig. 4b). The reason may be that the large gas evolution modifies the internal electrolyte transport pathways or changes the accessibility of the catalytically active surfaces in the electrode.

As a further test of the operation of the battolyser we applied various rapidly changing charge–discharge cycles (Fig. 5 and ESI,† Fig. S3). Such a test may mimic the application as a peak saving battery and electrolyser that experiences a high renewable electricity input (charge/electrolysis peak) interspaced with high electricity demand when the renewable electricity has shortages (discharge peak). As can be seen in Fig. 5, the battery and gas production functionalities of the cell follow the applied currents directly without delay, which is an asset compared to *e.g.* conventional electrolysers. Most remarkably in the ESI,† Fig. S3 the average potentials during fast charge and discharge switching come closer together, which means a higher electrical efficiency $\eta_{battery}$ during these rapidly varying currents; *i.e.* no adverse effects of switching but rather a positive effect.

The electrolysis potential as a function of current and temperature of a charged battolyser is shown in Fig. 6. Higher temperatures lead to lower ionic resistance and lower cell potential, increasing efficiency. The potential increases about 160 mV for a factor 10 higher current; this is a similar increase to that observed for advanced alkaline electrolysers at ~20 mA cm^{-2} current density.[19] We limited the test temperature to

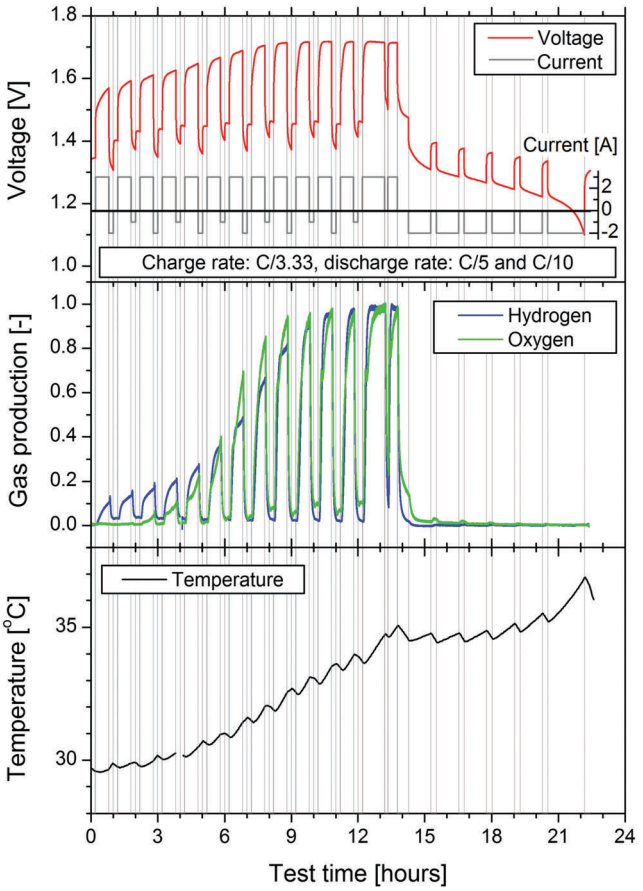

Fig. 5 Intermittent battolyser use. (top) Sequence of intermittent charge, discharge and rest steps that shows the switching capabilities of current insertion followed by immediate current withdrawal, rests and electrolytic gas evolution. (middle) The measured hydrogen and oxygen yields. (bottom) The temperature of the insulated cell following the instantaneous heating from residual overpotential losses due to Ohmic resistances.

40 °C preventing potential long term reduced stability issues of the iron electrode.[20] At the lowest currents, potentials below the thermoneutral potential of 1.48 V, but above the OCV of 1.37 V of the Ni–Fe battery are reached. Such electrolysis below the thermoneutral potential is possible because additional heat comes from the environment. In the normal electrolyser hydrogen production temperatures of 65–150 °C[11,21] are required and currents up to 400 mA cm^{-2} electrode surface area are applied in compromise between investment costs and operating efficiency (typically 71%[9]). The battolyser is operated with currents matching the normal (dis)charge rates of the battery active electrode mass and surface area, now reaching up to 20 mA cm^{-2} (Fig. 6). These same moderate currents split water efficiently at higher states of charge near room temperature, without any precious metal catalysts. These relatively moderate conditions mean a prolonged lifetime for all components. The operational flexibility exceeds these current limits, however: tests have been performed up to 100 mA cm^{-2} with an efficiency close to 80% at a device temperature well below 40 °C (see the ESI,† Fig. S6). Such efficiency is thus high compared to alkaline electrolysers.

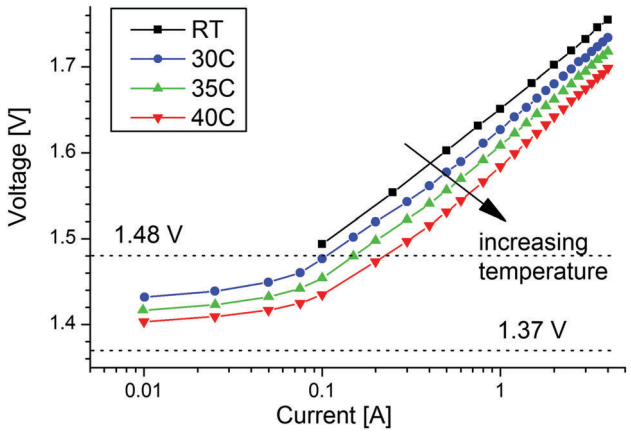

Fig. 6 Electrolysis full cell potential. Electrolysis potential dependence on applied current for several temperatures. The total external electrode surface area is 216 cm^2 and current densities of up to 20 mA cm^{-2} are reached.

Coming back to the small 7 mV reduction of the electrolysis potential observed in Fig. 4a we can now estimate that at a certain state of charge about 11% more current will be spent on electrolysis than on battery charging due to this 7 mV reduction. This is in line with the magnitude of the change of the battery discharge capacity after a fixed 24.0 A h charge insertion in Fig. 4a. The way in which the current is divided over the battery and the electrolyser (Fig. 3 and the ESI,† Fig. S2b) is thus slightly changed.

Energy density

The volumetric energy density in W h L^{-1} is relevant for the footprint that is occupied by an energy storage technology for stationary storage.[22] For the Ni–Fe based battery capabilities of the battolyser one can calculate the energy density of the cell, including the electrode materials but excluding external components such as electronics, water and gas treatment facilities (which are similar to an alkaline electrolyser). The theoretical energy density of the $Ni(OH)_2$ and $Fe(OH)_2$ electrode materials equals 1031 W h L^{-1} when using only the densities of the materials and an OCV of 1.37 V. An energy density of around 130–250 W h L^{-1} can be estimated as a practical limit taking into account that possibly a maximum of 20–30% of the cell volume may be occupied with active materials and the rest by the conductive construction and the electrolyte and gas flow areas, and also by taking into account the overpotentials for battery charge and discharge. The current experimental cell already reaches ~100 W h L^{-1}. Such energy density may be compared with liquid sodium–sulphur batteries (150–250 W h L^{-1}), lead-acid batteries (50–80 W h L^{-1}), lithium ion batteries (200–600 W h L^{-1}), or vanadium redox-flow batteries (16–33 W h L^{-1}).[23] In addition to the battery capabilities, however, the battolyser has the electrolyser capabilities that enable an unlimited additional W h to be stored in the form of hydrogen based fuels.

Stability

The findings of durability and flexibility are impressive since modern batteries will be rapidly destroyed by overcharging

and/or deep discharging, as well as loose the overcharge energy. Lithium ion batteries suffer from electrolyte decomposition during overcharging,[24] while nickel–metal hydride and lead-acid batteries suffer mainly from detrimental corrosion effects during overcharge and deep discharge.[25,26] The exceptional stability here will be related to the fact that the Ni and Fe based electrodes operate between the thermodynamically stable phases in their Pourbaix diagrams.[8,27] Apparently during the electrolysis mode at the negative electrode one can only reduce water to H_2 or reactivate iron hydroxides and oxides (when formed during deep discharge) to become Fe. The internal surface area of the electrode is sufficient for efficient HER and for reforming $Fe(OH)_2$ during discharge. At the positive electrode any $Ni(OH)_2$ which is oxidised to NiOOH or overcharged to γ-NiOOH[28–30] will readily revert to $Ni(OH)_2$ during discharge. Such intrinsic stable points of return during charge (Fe) or discharge ($Ni(OH)_2$, $Fe(OH)_2$) will enhance the stability of the electrodes during prolonged electrolysis operation and deep discharge. The switching tests shown in Fig. 5 and ESI,† Fig. S3 indicate that the cell potential rapidly relaxes to around an OCV of 1.37 V. Such a finding indicates that the active electrode materials still show the potentials corresponding to discharging NiOOH and Fe. The prolonged electrolysis does not lead to *e.g.* further oxidation of the Ni electrode to *e.g.* NiO_2.

The natural position of the electrode materials in their Pourbaix diagrams also account for the high efficiency of water splitting since the individual electrode potentials are close to the potentials for water splitting and the overall full cell potential (OCV = 1.37 V) is very close to 1.48 V, the thermoneutral potential required for water splitting.

Concluding remarks

The integration of a Ni–Fe battery and an alkaline electrolyser in one single device reaches high energy efficiencies of 80–90%, high compared to the individual Ni–Fe battery (~60–70%[7,31]) and alkaline electrolyser (typically up to 71% with respect to HHV[4,9]), and up to ~50% higher utilisation of the active battery material. The energy density of the battery capacity may reach values of up to 250 W h L^{-1} after optimisation. When only looking to the battery round trip efficiency in cycles without significant overcharging one sees efficiencies of ~80–83% (plus an additional percentage H_2, Fig. 3 and ESI,† Fig. S4), which may be compared to lithium ion batteries that are considered to have the highest efficiency, 90–94%, vanadium redox batteries, 65–70%, and liquid sodium–sulphur batteries, 75–80%.[2,10] Since the device can charge, perform electrolysis, discharge, and efficiently switch between those, it will have a very high utilisation degree and excellent flexibility that can be matched to demand. The combination of earth abundant Ni–Fe elements stores electricity as a battery, and splits water without noble metal catalysts which are in use in alkaline and PEM electrolysers.[12,32] The operation appears to be extremely durable, due to the position of the battery potentials close to the potentials needed for thermoneutral water splitting, and uniquely efficient. In this way heat losses in the battolyser charging are used partially for electrolysis, enhancing efficiency especially for the part of the hydrogen produced while the potential is close to the thermoneutral potential. The battolyser enables high power-to-power battery efficiency and can provide high power-to-fuel efficiency as well: battolyser electrolysis efficiency of up to 90% combined with industrial ammonia synthesis[13] may enable up to 80% (0.9 × 0.9) power to carbon neutral liquid fuel efficiency. The battolyser requires an amount of about 0.868 kg active Fe and 1.825 kg active Ni electrode material for storing 1 kW h of electricity in the battery functionality and the capability for unlimited hydrogen generation, which is not prohibitively expensive (<20 dollar; raw materials cost). Also a low cost water based electrolyte is used. We believe that these advantages of the integrated device will lead to reduced cost and a long lifetime compared to solutions using separate batteries and electrolysers, while the complexity of the infrastructure is essentially similar to an alkaline electrolyser, *i.e.* requires investments and operation similar to an electrolyser alone but with the double functionality.

Experimental section

Battolyser

A picture of the integrated battery electrolyser or the battolyser is shown in the ESI,† Fig. S1. The electrodes are produced using the technology description in ref. 31 and 33. $Ni(OH)_2$ is precipitated from a nickel sulfate solution, using concentrated NaOH. The $Ni(OH)_2$ precipitate is filtered, washed and dried at 120 °C. The dry hydroxide is ground with a 13 wt% graphitic carbon conductive additive, compacted and collected in perforated pockets of nickel coated steel. The iron electrode is produced from finely ground magnetite (Fe_3O_4), pure iron and 2 wt% of the graphitic carbon conductive additive plus a 10 wt% NaCl pore former. After compaction and sintering at 700 °C the pore former is dissolved and the electrode material is collected in perforated pockets of nickel coated steel. X-ray diffraction characterisation of the initial and activated material is shown in the ESI,† Fig. S8. The electrodes are separated from each other using state of the art gas separation membranes (Zirfon-Perl-UTP500 from Agfa Specialty Products). These membranes are known for their low resistance for ionic transport and stability of up to 110 °C (Zirfon[17]). A 4.5 molar potassium hydroxide electrolyte with 1.5 molar sodium hydroxide and 0.05 molar lithium hydroxide is utilised as described in ref. 31 and 33. Some tests were performed to observe if large effects of LiOH in the electrolyte on the potentials during electrolysis would be present (ESI,† Fig. S5).

Galvanostatic cycling

Various charge insertion and withdrawal experiments were programmed on a multichannel Maccor 2000 battery cycling system for total 7 different cells. The experiments leading to

Fig. 4 were performed independently ~~of~~ four different cells to check reproducibility and long term performance.

A cycle is counted from full discharge to full discharge. Fig. 4 and ESI,† Fig. S4 depict the chronological record of a cell. Various partial (over/dis)charge programs in between full discharges add up, so when there are many partial discharges and recharges before a final full discharge the aggregated (dis)charge in that cycle can be much larger than the nominal capacity (see the ESI,† Fig. S3 for a selection of performed cycles and the ESI,† Table S1 for additional data to these cycles). The graphs of Fig. 4 and Fig. S4 (ESI†) may seem spiky. This appearance originates in the diversity of tests applied to check the applicability of the battolyser as a renewable energy storage solution.

The charge rates that are often mentioned for battery charging are defined as follows: a charge rate of C/x means that the applied current corresponds to the insertion of the full nominal capacity in x hours.

Energy efficiency of battolyser discharge plus gas generation

The energy efficiency η_{total} for each charge and electrolysis and the subsequent discharge cycle is calculated from the equations:

$$\eta_{\text{total}} = \eta_{\text{battery}} + \eta_{\text{electrolyser}} \quad (5)$$

$$\eta_{\text{battery}} = \frac{\int_{t_c}^{t_c+t_{dc}} V_{dc} I_{dc} \mathrm{d}t}{\int_0^{t_c} V_c I_c \mathrm{d}t} \quad (6)$$

$$\eta_{\text{electrolyser}} = \frac{\int_0^{t_c+t_{dc}} H_{el} I_{el} \mathrm{d}t}{\int_0^{t_c} V_c I_c \mathrm{d}t} \quad (7)$$

V_c and I_c are the applied experimental cell voltage and current during the charge and electrolysis cycle with duration t_c, V_{dc} and I_{dc} are the experimental discharge voltage and current during the discharge time t_{dc}, I_{el} the current for electrolysis (and hydrogen evolution induced battery self-discharge) with an energy yield corresponding to the thermo neutral potential H_{el}. The H_{el} equals 1.48 V at RT while $2eH_{el}$ equals the higher heating value (HHV) of hydrogen of −286 kJ mol^{-1} H_2.

In Fig. S2a (ESI†) an illustration of the energy efficiency is shown graphically. In Tables S1–S3 (ESI†), explicit numeric examples are given for experimental energy efficiencies of several experiments. Of further interest for the temperature of the cell is the power generated as heat due to the losses. This power is the sum of ohmic losses in the battery function, which equal the absolute value $|V - 1.37|I_{dc}$, and the resulting losses in electrolysis, which equal $(V - 1.48) \times I_{el}$. The electrolysis losses can be positive or negative at very low currents (see remarks in relation to Fig. 6).

Below we show that the faradaic (or coulombic) efficiency equals 100% within the experimental accuracy of 0.5%. At this 100% faradaic efficiency the total charge C_c inserted in the battery electrolyser equals the charge used for electrolysis C_{el} plus the integrated current discharge C_{dc}:

$$C_c = \int_0^{t_c} I_c \mathrm{d}t = \int_0^{t_c+t_{dc}} I_{el} \mathrm{d}t + \int_{t_c}^{t_c+t_{dc}} I_{dc} \mathrm{d}t = C_{el} + C_{dc} \quad (8)$$

Note that the electrolysis yield C_{el} also includes the gas production during (self) discharge (if any).

The ionic resistance of the gas separation diaphragm was determined by measuring in a battolyser with and without the diaphragm in place. At the highest current density used an additional potential of ~10 mV was recorded, which corresponds to an energy efficiency loss of less than ~1%. Such small additional overpotential can be mitigated by a small change in operation temperature. Fig. 3b shows the measured discharge capacity and electrolysis yield as a function of the total charge insertion. The curves are the result of fitting with the following equations for C_{dc} and C_{el}, where the battery capacity saturates at $Ccap$:

$$C_{dc}(C) = C_{cap}\left(\frac{2}{1+\exp\left(-2\frac{C}{C_{cap}}\right)} - 1\right) \quad (9)$$

$$C_{el}(C) = C - C_{cap}\left(\frac{2}{1+\exp\left(-2\frac{C}{C_{cap}}\right)} - 1\right) \quad (10)$$

The charge is expressed in the unit [Coulomb] or [A h]. The function (5) above is a logistic function used more often for reactions where one of the reactants is limited (in this case the Ni electrode is limiting).[34] The fits in Fig. 3b describe the experimental data accurately. The instantaneous charge insertion in the two processes – either battery charging or electrolysis – at a certain moment, when a total charge current $I = \mathrm{d}C/\mathrm{d}t$ is applied, can be calculated from the derivatives of the equations for C_{dc} and C_{el} with respect to time:

$$\frac{\mathrm{d}C_{dc}(C)}{\mathrm{d}t} = I_{dc}(C) = \left(\frac{4\exp\left(-2\frac{C}{C_{cap}}\right)I}{\left(1+\exp\left(-2\frac{C}{C_{cap}}\right)\right)^2}\right) \quad (11)$$

and

$$\frac{\mathrm{d}C_{el}(C)}{\mathrm{d}t} = I_{el}(C) = I - \left(\frac{4\exp\left(-2\frac{C}{C_{cap}}\right)I}{\left(1+\exp\left(-2\frac{C}{C_{cap}}\right)\right)^2}\right) \quad (12)$$

$$\frac{\mathrm{d}C_{dc}(C)}{\mathrm{d}t} + \frac{\mathrm{d}C_{el}(C)}{\mathrm{d}t} = I_{dc}(C) + I_{el}(C) = I \quad (13)$$

Eqn (11) and (12) give the yield for either battery charge or electrolysis at a total applied charge current I, depending on the state of charge C/C_{cap} of the battery. ESI,† Fig. S2b shows the resulting curves for I_{dc}/I and I_{el}/I as a function of the total inserted charge. The saturation capacity C_{cap}, which is dependent on the available electrode material, is with 14.5 A h significantly larger than what we consider the nominal capacity of 10 A h of the battery. This is because the battery is normally considered to be full when the evolved gas is still small (Fig. 3b)

and then does not use the available electrode material as fully as the battolyser does; C_{cap} is significantly larger than the so defined nominal capacity therefore.

Water refilling, quantitative gas evolution, and faradaic efficiency

Demineralised water from a Merck Milli-Q Plus 185 water purification system was used for replenishing the electrolyte. The actual water loss was determined by weight after – on average – five individual completed cycles. In Fig. 4b the total inserted charge C_c minus the battery discharge C_{dc} is used to determine the amounts of electrolysis C_{el}, assuming 100% faradaic (or coulombic) efficiency. The result is compared with the actual lost (and subsequently replenished) amounts of demineralised water that are expressed in a capacity as well (1 g of water corresponds to $2F/(18.02 \times 3600)$ A h where F is the Faraday constant of 96 485 s A mol^{-1} and the molar mass of water equals 18.02 g mol^{-1}). This already gives for all cycles together that the faradaic efficiency is close to 100%.

As a second independent verification of the faradaic efficiency the rate of the gas evolution was determined volumetrically for the charged battolyser at several constant applied currents using calibrated gas syringes (Poulten–Graf, Fortuna 100 ml). The volumes of gas measured in ml s^{-1} are within 0.5% agreement with corresponding theoretical values for the ambient temperature and pressure. Combining the charge insertion with the discharge capacity and the water loss and gas volume evolutions we come to the conclusion that the faradaic efficiency is 100 ± 0.5% based on the experimental accuracies. With this outcome it is justified to use 100% faradaic efficiency in our energy efficiency calculations.

Gas characterisation and separation

The separate channels of hydrogen and oxygen were analysed during operation using a calibrated quantitative gas analysis system with a sensitive Hiden 3F-PIC series Quadrupolar Mass Spectrometer for detection. During these gas measurements an argon carrier gas flow was administered over the exit of cell gas. There is hardly any detectable O_2 in the hydrogen channel and hardly any detectable H_2 in the oxygen channel.

Thermally insulated cell

The battolyser was insulated as far as possible by using styrofoam insulation. Still the electronic leads and also the argon gas flow for the gas measurements cause heat flows between cells and the environment. Temperature changes in Fig. 3a and 5 are the resultant of the overpotentials and the thermal losses through the insulation. Measurements were also performed on uninsulated cells in temperature regulated ovens with temperature regulation to ±0.1 °C.

Lithium in the electrolyte

Lithium hydroxide (LiOH) is normally not utilised in alkaline electrolysis, but it is used in Ni–Fe batteries. To observe if detrimental effects on the electrolysis efficiency may be present we varied the LiOH concentration which was added to a 21 wt% KOH solution from 0 (pure KOH) to 0.5 and 1.0 mol L^{-1}. In the ESI,† Fig. S5, results for a large range of current insertions (in A h) are shown. Although the efficiency of electrolysis increases about 0.5% without addition of LiOH, such an increase is less than for instance the effects of temperature variation (~4%). In view of this limited impact and the low 0.05 molar LiOH concentration applied for battery operation this concentration was maintained throughout the experiments.

Competing financial interests

The authors declare no competing financial interests.

Author contributions

F. M. devised the research project, B. W. worked out the research methodology and performed the experiments, B. W., H. S., J. M. and F. M. designed the experimental setup, H. S., J. M. and F. O. gave experimental support, B. W. and F. M. analysed the data, F. M. and B. W. wrote the manuscript, F. M. supervised the project.

Acknowledgements

We thank B. Dam and L. D. A. Siebbeles for discussion of the manuscript.

Notes and references

1 M. Armand and J. M. Tarascon, *Nature*, 2008, **451**, 652–657.
2 B. Dunn, H. Kamath and J.-M. Tarascon, *Science*, 2011, **334**, 928–935.
3 A. Zuttel, A. Remhof, A. Borgschulte and O. Friedrichs, *Philos. Trans. R. Soc., A*, 2010, **368**, 3329–3342.
4 J. D. Holladay, J. Hu, D. L. King and Y. Wang, *Catal. Today*, 2009, **139**, 244–260.
5 N. Armaroli and V. Balzani, *Energy Environ. Sci.*, 2011, **4**, 3193–3222.
6 F. M. Mulder, *J. Renewable Sustainable Energy*, 2014, **6**, 033105.
7 D. Linden and T. B. Reddy, *Handbook of Batteries Third Edition*, McGraw-Hill, 2001.
8 K. Vijayamohanan, T. S. Balasubramanian and A. K. Shukla, *J. Power Sources*, 1991, **34**, 269–285.
9 K. Zeng and D. K. Zhang, *Prog. Energy Combust. Sci.*, 2010, **36**, 307–326.
10 M. A. Pellow, C. J. M. Emmott, C. J. Barnhart and S. Benson, *Energy Environ. Sci.*, 2015 8, 1938 - 1952
11 A. Ursua, L. M. Gandia and P. Sanchis, *Proc. IEEE*, 2012, **100**, 410–426.
12 J. A. Herron, J. Kim, A. A. Upadhye, G. W. Huber and C. T. Maravelias, *Energy Environ. Sci.*, 2015, **8**, 126–157.
13 J. R. Jennings, *Catalytic ammonia synthesis: fundamentals and practice*, Springer Science & Business Media, 2013.
14 C. C. L. McCrory, S. Jung, I. M. Ferrer, S. M. Chatman, J. C. Peters and T. F. Jaramillo, *J. Am. Chem. Soc.*, 2015, **137**, 4347–4357.

15 G. A. Snook, N. W. Duffy and A. G. Pandolfo, *J. Power Sources*, 2007, **168**, 513–521.
16 M. K. Ravikumar, T. S. Balasubramanian, A. K. Shukla and S. Venugopalan, *J. Appl. Electrochem.*, 1996, **26**, 1111–1115.
17 P. Vermeiren, J. P. Moreels, A. Claes and H. Beckers, *Int. J. Hydrogen Energy*, 2009, **34**, 9305–9315.
18 R. C. Saltat, *Nickel-iron battery system safety*, Report NASA-CR-173937, JPL-9550-910, NAS 1.26:173937, DOE/CS-54209/17, Eagle-Pichler Industries, Inc., NASA STI, 1984.
19 S. Marini, P. Salvi, P. Nelli, R. Pesenti, M. Villa, M. Berrettoni, G. Zangari and Y. Kiros, *Electrochim. Acta*, 2012, **82**, 384–391.
20 L. Ojefors, *J. Electrochem. Soc.*, 1976, **123**, 1139–1144.
21 D. Pletcher and X. H. Li, *Int. J. Hydrogen Energy*, 2011, **36**, 15089–15104.
22 Y. Gogotsi and P. Simon, *Science*, 2011, **334**, 917–918.
23 H. Chen, T. N. Cong, W. Yang, C. Tan, Y. Li and Y. Ding, *Prog. Nat. Sci.*, 2009, **19**, 291–312.
24 N. S. Choi, Z. H. Chen, S. A. Freunberger, X. L. Ji, Y. K. Sun, K. Amine, G. Yushin, L. F. Nazar, J. Cho and P. G. Bruce, *Angew. Chem., Int. Ed.*, 2012, **51**, 9994–10024.
25 F. Feng, M. Geng and D. O. Northwood, *Int. J. Hydrogen Energy*, 2001, **26**, 725–734.
26 F. Y. Cheng, J. Liang, Z. L. Tao and J. Chen, *Adv. Mater.*, 2011, **23**, 1695–1715.
27 A. I. Demidov and E. N. Volkova, *Russ. J. Appl. Chem.*, 2009, **82**, 1498–1500.
28 J. Desilvestro, D. A. Corrigan and M. J. Weaver, *J. Electrochem. Soc.*, 1988, **135**, 885.
29 D. A. Corrigan and S. L. Knight, *J. Electrochem. Soc.*, 1989, **136**, 613–619.
30 A. Van der Ven, D. Morgan, Y. S. Meng and G. Ceder, *J. Electrochem. Soc.*, 2006, **153**, A210–A215.
31 S. U. Falk and A. J. Salkind, *Alkaline storage batteries*, John Wiley & Sons, 1969.
32 D. Stolten, *Hydrogen Science and Engineering: Materials, Processes, Systems and Technology*, John Wiley & Sons, 2016, vol. 2.
33 R. Kinzelbach, *Stahlakkumulatoren*, VARTA Batterie AG, Hannover, 1974.
34 N. W. Loney, *Applied mathematical methods for chemical engineers*, CRC Press, 2015.